Research Paper
Computational Methods for Differential Equations
http://cmde.tabrizu.ac.ir
Vol. *, No. *, *, pp. 1-18
DOI:10.22034/cmde.2025.62206.2727

Comparative numerical analysis of rotating flow of a stretching sheet with hall current, thermal diffusion and heat source for an MHD base fluid, casson nanofluid, and hybrid nanofluid

Mohana Ramana Ravuri[1], Ch. Maheswari[1], Raghunath Kodii[2,*], and Sridevi Dandu[3,*]

[1]Department of Mathematics, Narasaraopeta Engineering College (Autonomous), Narasaraopet-522601, Andhra Pradesh, India.

[2]Department of Humanities and Sciences, St. Johns College of Engineering and Technology (Autonomous), Yemmiganur-518360, Andhra Pradesh, India.

[3]Department of Engineering Mathematics & Humanities, S.R.K.R. Engineering College, Bhimavaram, West Godavari District, Andhra Pradesh, India.

Abstract

This work examines the heat and mass transfer characteristics of MHD rotating $Fe_3O_4 - Al_2O_3/H_2O$ hybrid nanofluid flow over a three-dimensional linear stretching surface. A comparative analysis has been carried out among the base fluid H_2O, $Al_2O_3 - H_2O$ Casson hybrid nanofluid and Fe3O4 $Fe_3O_4 - Al_2O_3/H_2O$ Casson hybrid nanofluid concerning velocity, temperature and concentration distributions, influenced by various parameters, including Thermal diffusion, heat source, thermophoresis, Brownian motion, Hall current, temperature ratio parameter, magnetic parameter, rotation parameter, thermal radiation. The system of nonlinear ordinary differential equations (ODEs) is derived from the set of nonlinear partial differential equations (PDEs) by employing similarity adaptations. Numerical solutions are obtained using the BVP-5C method implemented in MATLAB with a shooting approach. Rising the thermophoresis parameter leads to heightened temperature and concentration profiles. Similarly, as Brownian motion values escalate, the temperature profile elevates while the concentration distribution reduces. Additionally, an increase in both the Hall parameter and the temperature ratio parameter correlates with a rise in the temperature profile. The local Nusselt number demonstrates a decline as the thermophoresis parameter and Brownian motion values increase. Moreover, the Sherwood number tends to ascend with higher Brownian motion values, while it tends to decrease with increasing thermophoresis parameter values. The temperature distribution of the hybrid nanofluid shows a notable increase compared to both the nanofluid and the base fluid under the influence of thermophoresis and Brownian motion characteristics. Conversely, the concentration gradient of the base fluid exceeds that of both the nanoliquid and hybrid nanoliquid when considering the same parameters. In accordance with Karl Pearson's approach, the coefficient of correlation reveals a perfect positive correlation, close to 1, between the current and previous outcomes of the Nusselt number.

Keywords. Thermal diffusion, Heat source, Thermophoresis, Brownian motion, Hall current, Joule heating.
2010 Mathematics Subject Classification. 65L05, 34K06, 34K28.

1. Introduction

In recent decades, scientists and researchers have focused their attention on the study of a new class of fluid known as a hybrid nanofluid. Fluids with a higher thermal conductivity than nanofluids and base fluid are known as hybrid nanofluids. Hybrid nanofluids are formed by diffusing two sorts of nanoparticles in the carrier liquid. Mechanically to improve the transmission of heat in a variety of engineering and manufacturing processes the hybrid nanoparticles energy transition has been devolved. The hybrid nanofluid has strong thermal reliability as compared to the classical and base liquid. The numerous applications of hybrid nanofluid in industries and engineering mechanisms are heat pumps, heat capacitors microelectronics, digital cooling, car radiators, nuclear power stations, coolant in writing and machine tools, chemical producers, nano drag shipments, automobile power creation, cancer treatment, and so

Received: 21 June 2024 ; Accepted: 08 September 2025.
∗ Corresponding author. Email: kraghunath25@gmail.com.

forth. Several studies on hybrid nanofluid being conducted by many researchers and scientists as a result of their significant applications. Shoaib et al. [36] considered the spinning flow of nanofluid flow with radiation effects inside the stretching surface and noticed a variation of rotation parameter for velocity profile. Hanaya et al. [3] explained the micropolar hybrid nanofluid flow toward the curved stretching surface containing SWCNT and MWCNT nanoparticles and applied the bvp4c-shooting scheme for the examination of their model results. Liaquat et al. [14] numerically computed the MHD hybrid nanofluid flow toward the shrinking surface for stability analysis and dual solutions and their problem consists of $Cu - Al_2O_3$–water the base fluid. They found that for increasing values of suction and radiation parameters temperature is enhanced (decrease) for both solutions. Shoaib et al.[37] scrutinized the phenomena of viscous dissipation in 3D MHD hybrid nanofluid flow via rotating disk. In this research work, it is noted that magnetic field reduced both the radial and azimuthal skin frictions coefficients. Ahmad et al. [2] pointed out the study of $Go+Silver(Ag)$ in Maxwell hybrid nanoliquid for the improvement of thermal performance. Their concluding remarks illustrated that the heat transition is improved through the addition of silver volume fraction with graphene oxide. Alhussain et al.[4] inspected the influence of variable viscosity in a blood-based two-dimensional Casson hybrid nanofluid through the stretching sheet by introducing a magnetic field perpendicular in a flow field. From this analysis, the authors have demonstrated that with the increment of nanomaterials concentration in the base fluid, the thermal expansion rate is increased but the specific heat capacity decreased. Sreedevi et al. [35] perceived a numerical study for gyrotactic microorganism's past over a swirling cylinder and examined that microorganism density is raised for Weissenberg number. In addition, Roy et al. [38] inspected the second-grade nanoliquid flow across an extending surface along with heat propagation. They reported that the heat flux is condensed but wall shear stress is improved through the variation of velocity ratio parameter. Magnetohydrodynamics (MHD) refers to the study of the behavior of electrically conductive fluids in the presence of magnetic fields, with applications in a wide range of engineering fields, including heat transfer, energy production, and biomedical engineering. MHD plays a critical role in various industrial applications such as the cooling of nuclear reactors, aerospace propulsion, and the design of efficient energy systems. Recent studies have expanded the understanding of MHD flows, including the effects of external factors such as Hall current, radiation absorption, and thermal diffusion on fluid dynamics. For instance, Katikala et al. [11] explored the impact of Hall current and Joule heating on MHD flow of second-grade fluid through porous media. Lavanya et al. [13] conducted a comprehensive study on Carreau nanofluid flow over an inclined vertical plate, focusing on heat transfer using the Cattaneo-Christov heat flux model. Pasha et al. [17] investigated the effects of rotational forces and thermal diffusion on unsteady MHD flow of viscoelastic fluid through porous media . Reddy et al. [32] analyzed the influence of thermo-physical effects and aligned magnetic fields on MHD convection in Casson fluids . Hussain et al. [9] studied the effects of non-Newtonian hybrid nanofluid flow in the presence of rotational forces over a stretched plate. Further, Valiveti et al. [39] examined heat and mass transfer in MHD Casson fluid flow with thermal diffusion and heat source effects . Prasad et al. [18] focused on Hall current and thermal diffusion in the unsteady MHD rotating flow of nanofluids . Additionally, Jyothi et al. [10] used a neural network-assisted analysis to study MHD boundary layer flow and thermal radiation effects on SWCNT nanofluids . Recent advancements also include Bhargava et al. [6] analyzing MHD mixed convection and radiation effects on hybrid nanofluid flow through porous media. Yadav et al. [34] examined the impact of temperature-dependent thermal conductivity and viscosity variations on the convection of Jeffrey fluid in rotating porous layers Thermal diffusion, also known as the Soret effect, refers to the phenomenon where a temperature gradient in a mixture leads to the migration of particles from higher to lower temperature regions. This effect plays a critical role in the heat and mass transfer processes of fluids, especially in nanofluids and magnetohydrodynamic (MHD) flows. In industrial and engineering applications, understanding thermal diffusion helps optimize processes such as cooling systems, chemical reactions, and energy management. Recent studies have examined the influence of thermal diffusion in various fluid systems. Raghunath et al. [19] explored the thermodynamic and buoyancy force effects of Cu and TiO_2 nanoparticles in engine oil flow, highlighting its importance in enhancing thermal conductivity. Zhang et al. [33] investigated the effects of thermo diffusion and diffusion-thermo on 3D-MHD mixed convection in a Darcy-Forchheimer Maxwell fluid. Further, Raghunath et al. [24] studied the MHD flow of Jeffrey fluid with thermal radiation, Hall current, and Soret effects, revealing critical insights into the behavior of such flows in porous media. Raju et al. [30] analyzed chemical radiation and Soret effects on unsteady MHD convective flow, underscoring the significant role of thermal diffusion in such flows. Additionally, studies by Reddy et al. [31]

Raghunath et al. [20, 25] have discussed studdy of Heat and Mass Transfer of an Unsteady Magnetohydrodynamic Nanofluid Flow Past a Vertical Porous Plate in the Presence of Chemical Reaction, Radiation and Soret Effects and Omar et al. [16] have provided valuable data on the impact of thermal diffusion in MHD nanofluid flows and the role of diffusion-thermo in improving heat transfer performance. Deepthi et al. [40] discussed recent development of heat and mass transport in the presence of hall, ion slip and thermo diffusion in radiative second grade material. Hall current is a phenomenon that occurs in electrically conductive fluids when subjected to a magnetic field, resulting in the generation of an electric field perpendicular to both the fluid's motion and the magnetic field. This effect significantly influences the flow characteristics, especially in magnetohydrodynamic (MHD) systems. Hall current is particularly relevant in applications involving high-temperature plasmas, energy conversion systems, and cooling technologies in nuclear reactors and aerospace systems. The effect of Hall current has been widely studied in various fluid systems, particularly in nanofluids and porous media flows. Recent studies by Raghunath et al. [28] have discussed rotating mixed convective Casson fluid flow past inclined porous plates with the effects of Hall and ion slip, radiation absorption, and diffusion thermo. Sunitha Rani et al. [28] studied unsteady MHD rotating mixed convective flow through an infinite vertical plate, considering Joule heating, thermal radiation, Hall current, and radiation absorption. Kommaddi et al.[7] explored heat and mass transfer on unsteady MHD chemically reacting rotating flow of Jeffrey fluid past inclined plates under the impact of Hall current, diffusion thermo, and radiation absorption. Raghunath et al.[26] investigated the Hall current and thermal radiation effects of 3D rotating hybrid nanofluid reactive flow via stretched plates with internal heat absorption. Raghunath et al. [27] processed unsteady MHD flow of a second-grade fluid through a porous medium in the presence of radiation absorption, diffusion thermo, Hall, and ion slip effects. Kumar et al. [12] presented a numerical analysis of magnetohydrodynamic Casson nanofluid flow with activation energy, Hall current, and thermal radiation. Aruna et al. [5] examined an unsteady MHD flow of a second-grade fluid passing through a porous medium, focusing on radiation absorption and the effects of Hall and ion slip. Raghunath and Ravuri [21] studied the Hall, Soret, and rotational effects on unsteady MHD rotating flow of a second-grade fluid through a porous medium, considering chemical reaction and aligned magnetic field. Raghunath et al. [22] analyzed Hall and ion slip radiative flow of chemically reactive second-grade fluid through porous saturated space via perturbation approach. Raghunath et al. [23] explored the effects of Soret, rotation, Hall, and ion slip on unsteady MHD flow of a Jeffrey fluid through a porous medium in the presence of heat absorption and chemical reaction. Obulesu et al. [41] discussed Hall current effects on MHD convective flow past a porous plate with thermal radiation, chemical reaction, and radiation absorption. Raghunath et al. [29] studied Hall effects on MHD convective rotating flow of second-grade fluid through a porous medium past an infinite vertical plate. The novelty of this study lies in its comprehensive comparative analysis of MHD rotating flow of a base fluid, Casson nanofluid, and hybrid nanofluid over a stretching sheet, incorporating the effects of Hall current, thermal diffusion, heat source, thermophoresis, and Brownian motion. While previous studies have primarily focused on individual fluid properties or isolated effects, this work combines several key factors such as Hall current, thermal radiation, and the interaction between thermophoresis and Brownian motion to provide a holistic understanding of fluid flow behavior in nanofluid systems. The use of the BVP-5C method and shooting approach in MATLAB for solving the derived nonlinear ordinary differential equations further enhances the accuracy and reliability of the numerical solutions. Notably, the paper also offers new insights into how the temperature and concentration distributions respond to varying Hall current, thermophoresis, and Brownian motion parameters in the context of hybrid nanofluid flow, which has not been extensively studied before. Additionally, the study's exploration of the Nusselt and Sherwood numbers, their dependence on the thermophoresis and Brownian motion parameters, and their correlation with previous outcomes using Karl Pearson's method, contribute to the novelty by quantifying the relationship between the heat and mass transfer rates in MHD nanofluid flows under complex thermal conditions.

2. Mathematical Formulation of the Problem

This investigation explores the behaviour of a three dimensional, incompressible hybrid nanofluid $(Fe_3O_4 - Al_2O_3/H_2O)$, nanofluid $(Fe_3O_4 - H_2O)$ and base fluid water (H_2O) flows under steady-state conditions as shown in Figure1. The fluids are laminar and consists of electrically conductive Fe_3O_4/Al_2O_3 nanoparticles with water as base fluid. The flow occurs over a stretching sheet with a constant angular velocity ω, while the nanoparticles travel at a consistent velocity $U_w = bx$. At first, a nanofluid $Fe_3O_4 - H_2O$ is formed by dispersing Fe_3O_4 nanoparticles

with a volume fraction denoted as ϕ_1 in the base fluid water. Subsequently, the nanofluid is further enhanced to create $Fe_3O_4 - Al_2O_3/H_2O$ hybrid nanofluid, by introducing Al_2O_3 with a high thermal conductivity and a specified volume fraction ϕ_2 into the $Fe_3O_4 - H_2O$ nanofluid. The plate experiences nonlinear thermal radiation, accompanied by a heat flux denoted as q_r. Additionally, uniform magnetic field with an intensity of B_0 and the presence of Hall current are applied perpendicularly to the plate. The temperature at the consistency and far away from the texture are symbolized by T_w and T_∞ respectively.

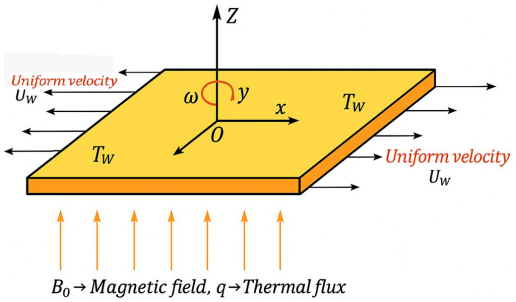

FIGURE 1. Geometry of the flow and coordinate system [8].

Under the stated assumptions, three dimensional non-linear technique of PDEs that encloses continuity, rate, dynamism and conservation can be expressed as follows (Elsaid et al. [8]):

$$\frac{\partial u}{\partial x} + \frac{\partial v}{\partial y} + \frac{\partial w}{\partial z} = 0. \tag{2.1}$$

$$\rho_{hnf}\left(u\frac{\partial u}{\partial x} + v\frac{\partial u}{\partial y} + w\frac{\partial u}{\partial z} - 2\omega v\right) = \mu_{hnf}\left(1 + \frac{1}{\beta}\right)\left(\frac{\partial^2 u}{\partial z^2}\right) - \frac{\sigma_{hnf}B_0^2}{(1+m^2)}(u - mv). \tag{2.2}$$

$$\rho_{hnf}\left(u\frac{\partial v}{\partial x} + v\frac{\partial v}{\partial y} + w\frac{\partial v}{\partial z} + 2\omega u\right) = \mu_{hnf}\left(1 + \frac{1}{\beta}\right)\left(\frac{\partial^2 v}{\partial z^2}\right) - \frac{\sigma_{hnf}B_0^2}{(1+m^2)}(v + mu). \tag{2.3}$$

$$\begin{aligned}(\rho C_p)_{hnf}\left(u\frac{\partial T}{\partial x} + v\frac{\partial T}{\partial y} + w\frac{\partial T}{\partial z}\right) &= k_{hnf}\left(\frac{\partial^2 T}{\partial z^2}\right) + \frac{\partial^2 T^4}{\partial z^2}\left(\frac{4\sigma^*}{3\alpha^*}\right) + \sigma_{hnf}B_0^2\left(u^2 + v^2\right) \\ &\quad + \tau\left[\frac{D_T}{T_\infty}\left(\frac{\partial T}{\partial z}\right)^2 + D_B\left(\frac{\partial C}{\partial z}\right)\left(\frac{\partial T}{\partial z}\right)\right] + Q_0(T - T_\infty).\end{aligned} \tag{2.4}$$

$$u\frac{\partial C}{\partial x} + v\frac{\partial C}{\partial y} + w\frac{\partial C}{\partial z} = \beta_{hnf}\frac{\partial^2 C}{\partial z^2} + \frac{D_M k_T}{T_M}\frac{\partial^2 T}{\partial z^2} - \xi_1(C - C_\infty)^n + \frac{D_T}{T_\infty}\left(\frac{\partial^2 T}{\partial z^2}\right). \tag{2.5}$$

Viscosity μ_{hnf}, density ρ_{hnf}, heat capacity $(\rho C_p)_{hnf}$, electrical conductivity σ_{hnf}, thermal conductivity k_{hnf} and Concentration diffusivity β_{hnf} of hybrid nanofluid are given in the following Table 1.

2.1. **Mathematical Formulation.** With the following boundary conditions (Elsaid et al. [12]):

$$\begin{aligned} &u = u_w, \quad v = 0, \quad w = 0, \quad T = T_w, \quad C = C_w \quad \text{at } z = 0. \\ &u \to 0, \quad v \to 0, \quad T \to T_\infty, \quad C \to C_\infty \quad \text{as } z \to \infty. \end{aligned} \tag{2.6}$$

In accordance with the Roseland approximation, the radiation flux includes the following:

$$q_r = -\frac{4\sigma^*}{3\alpha^*}\frac{\partial T^4}{\partial z}. \tag{2.7}$$

TABLE 1. Thermophysical properties of Al_2O_3–H_2O nanofluid [1, 8, 15, 29].

Property	Expression
Viscosity (μ)	$\mu_{nf} = \frac{\mu_f}{(1-\phi_2)^{2.5}}$
Density (ρ)	$\rho_{nf} = (1-\phi_2)\rho_f + \phi_2\rho_{S_2}$
Heat capacity (ρC_p)	$(\rho C_p)_{nf} = (1-\phi_2)(\rho C_p)_f + \phi_2(\rho C_p)_{S_2}$
Thermal conductivity (k)	$\frac{k_{nf}}{k_f} = \frac{k_{S_2} + 2k_f - 2\phi_2(k_f - k_{S_2})}{k_{S_2} + 2k_f + \phi_2(k_f - k_{S_2})}$
Electrical conductivity (σ)	$\frac{\sigma_{nf}}{\sigma_f} = \frac{\sigma_{S_2} + 2\sigma_f - 2\phi_2(\sigma_f - \sigma_{S_2})}{\sigma_{S_2} + 2\sigma_f + \phi_2(\sigma_f - \sigma_{S_2})}$

TABLE 2. Thermophysical properties of Fe_3O_4–Al_2O_3/H_2O hybrid nanofluid [1, 8, 15, 29].

Property	Expression
Viscosity (μ)	$\mu_{hnf} = \frac{\mu_f}{(1-\phi_1)^{2.5}(1-\phi_2)^{2.5}}$
Density (ρ)	$\rho_{hnf} = (1-\phi_2)\{(1-\phi_1)\rho_f + \phi_1\rho_{S_1}\} + \phi_2\rho_{S_2}$
Heat capacity (ρC_p)	$(\rho C_p)_{hnf} = (1-\phi_2)\{(1-\phi_1)(\rho C_p)_f + \phi_1(\rho C_p)_{S_1}\} + \phi_2(\rho C_p)_{S_2}$
Thermal conductivity (k)	$\frac{k_{hnf}}{k_{bf}} = \frac{ks_2 + 2k_{bf} - 2\phi_2(k_{bf} - ks_2)}{ks_2 + 2k_{bf} + \phi_2(k_{bf} - ks_2)}$, where $\frac{k_{bf}}{k_f} = \frac{ks_1 + 2k_f - 2\phi_1(k_f - ks_1)}{ks_1 + 2k_f + \phi_1(k_f - ks_1)}$
Electrical conductivity (σ)	$\frac{\sigma_{hnf}}{\sigma_{bf}} = \frac{\sigma_{S_2} + 2\sigma_{bf} - 2\phi_2(\sigma_{bf} - \sigma_{S_2})}{\sigma_{S_2} + 2\sigma_{bf} + \phi_2(\sigma_{bf} - \sigma_{S_2})}$, where $\frac{\sigma_{bf}}{\sigma_f} = \frac{\sigma_{S_1} + 2\sigma_f - 2\phi_1(\sigma_f - \sigma_{S_1})}{\sigma_{S_1} + 2\sigma_f + \phi_1(\sigma_f - \sigma_{S_1})}$
Concentration diffusivity (β)	$\beta_{hnf} = (1-\phi_1)(1-\phi_2)\beta_f$

The similitude mutations are characterized as (Elsaid et al. [12]):

$$u = bxf'(\eta), \quad v = bxg(\eta), \quad w = -\sqrt{b\nu_f}f(\eta), \eta = \sqrt{\frac{b}{\nu_f}}z$$
$$T = T_\infty + (T_w - T_\infty)\theta(\eta), \quad C = C_\infty + (C_w - C_\infty)\phi(\eta). \tag{2.8}$$

Following are the non-dimensional parameters:

$$\lambda = \frac{\omega}{b}, \quad \nu_f = \frac{\mu_f}{\rho_f}, \quad M = \frac{\sigma_f B_0^2}{b\rho_f}, \quad \Pr = \frac{\nu_f(\rho C_p)_f}{k_f},$$
$$Ec = \frac{u_w^2\rho_f}{(\rho C_p)_f(T_w - T_\infty)}, \quad \theta_w = \frac{T_w}{T_\infty}, \quad u_w = bx, \quad Sc = \frac{\nu_f}{D_B},$$
$$Rc = \frac{\xi_1(C - C_\infty)^{n-1}}{b}, \quad Nt = \frac{D_T\tau(T_w - T_\infty)}{\nu_f T_\infty}, \quad Q_0 = \frac{Q}{(\rho C_p)_f}, \quad Nb = \frac{D_B\tau(C_w - C_\infty)}{\nu_f},$$
$$Sr = \frac{D_M k_T(T_w - T_\infty)}{\nu_f T_M(C_w - C_\infty).} \tag{2.9}$$

Exploiting the similitude mutations Equation (2.8) and the non-dimensional specifications Equation (2.9), Equation (2.1) is inherently fulfilled, while Equations (2.2), (2.3), (2.4), and (2.5) are transformed into the subsequent equations:

$$\frac{l_4}{l_1}\left(1+\frac{1}{\beta}\right)f'''-f'^2+ff''+2\lambda g-\frac{l_5}{l_1}\frac{M}{1+m^2}(f'-mg)=0. \tag{2.10}$$

$$\frac{l_4}{l_1}\left(1+\frac{1}{\beta}\right)g''+fg'-f'g-2\lambda f'-\frac{l_5}{l_1}\frac{M}{1+m^2}(g+mf')=0. \tag{2.11}$$

$$\left(1+\frac{Rd}{l_3}\left[1+(\theta_w-1)\theta\right]^3\right)\theta''+\Pr\frac{l_2}{l_3}f\theta'+\frac{3Rd}{l_3}\left[1+(\theta_w-1)\theta\right]^2(\theta_w-1)\theta'^2+\frac{l_5}{l_3}MEcPr(f'^2+g^2)+\frac{Pr}{l_3}Q\theta + \frac{Pr}{l_3(\rho C_p)_f}(Nt\theta'^2+Nb\phi'\theta')=0. \tag{2.12}$$

$$\phi''+\frac{Sc}{l_6}(f\phi'-Rc\phi+Sr\theta'')+\frac{1}{l_6}\frac{Nt}{Nb}\theta''=0. \tag{2.13}$$

where

$$l_1=\frac{\rho_{hnf}}{\rho_f},\qquad l_2=\frac{(\rho C_p)_{hnf}}{(\rho C_p)_f},\qquad l_3=\frac{k_{hnf}}{k_f},\qquad l_4=\frac{\mu_{hnf}}{\mu_f},\qquad l_5=\frac{\sigma_{hnf}}{\sigma_f},\qquad l_6=\frac{\beta_{hnf}}{\beta_f}.$$

The transformed boundary conditions are:

$$\begin{aligned} &f(0)=0, && f'(0)=1, && g(0)=0, && \theta(0)=1, && \phi(0)=1,\\ &f'(\eta)\to 0, && g(\eta)\to 0, && \theta(\eta)\to 0, && \phi(\eta)\to 0 && \text{as } \eta\to\infty. \end{aligned} \tag{2.14}$$

The problem focuses on the relevant physical quantities, the Skin friction coefficient along x and y-axis C_{fx}, C_{fy} ($\sqrt{Re}\,C_{fx}$, $\sqrt{Re}\,C_{fy}$), local Nusselt number (Nu_x) and Sherwood number (Sh_x). The final Dimensionless forms of physical excesses of appeal involving in this model are given by [12, 37]

$$\sqrt{Re}C_{fx}=l_4f''(0),\qquad \sqrt{Re}C_{fy}=l_4g'(0),\qquad \frac{Nu_x}{\sqrt{Re}}=-(l_3+Rd\theta_w^3)\theta'(0),\qquad \frac{Sh_x}{\sqrt{Re}}=-l_3\phi'(0). \tag{2.15}$$

where $Re=\frac{U_wx}{\nu_f}$ is the restricted Reynolds number.

3. Method of Solution

A numerical investigation was carried out on a system of non-linear ordinary differential Equations (2.10) to (2.13) alongside their associated boundary conditions given in Equation (2.14) using the BVP-5C shooting technique within the MATLAB environment. By incorporating extra variables, the interconnected non-linear ODEs are converted into a collection of linear first-order ODEs, offering a notable advantage of this approach.

First, write the non-linear ODEs Equations (2.10) to (2.13) in the following form:

$$f'''=\left(\frac{l_1}{l_4}\right)\left(\frac{1+\beta}{\beta}\right)\left[f'^2-ff''-2\lambda g\right]+\left(\frac{l_5}{l_4}\right)\frac{M}{1+m^2}\left(f'-mg\right), \tag{3.1}$$

$$g''=\left(\frac{1+\beta}{\beta}\right)\left(\frac{l_1}{l_4}\right)\left[f'g-fg'+2\lambda f'\right]+\left(\frac{l_5}{l_4}\right)\frac{M}{1+m^2}\left(g+mf'\right), \tag{3.2}$$

$$\theta''=-\frac{1}{1+\frac{Rd}{l_3}\left[1+(\theta_w-1)\theta\right]^3}\left[\Pr\frac{l_2}{l_3}f\theta'+\frac{3Rd}{l_3}\left[1+(\theta_w-1)\theta\right]^2(\theta_w-1)\theta'^2 + \frac{l_5}{l_3}MEc\Pr\left(f'^2+g^2\right)-\frac{\Pr}{l_3}Q\theta+\frac{\Pr}{l_3(\rho C_p)_f}\left(Nt\,\theta'^2+Nb\,\phi'\theta'\right)\right], \tag{3.3}$$

$$\phi''=-\frac{Sc}{l_6}\left(f\phi'-Rc\,\phi+Sr\,\theta''\right)-\frac{1}{l_6}\frac{Nt}{Nb}\theta''. \tag{3.4}$$

TABLE 3. Thermophysical properties of Fe_3O_4, Al_2O_3, and H_2O [8].

Properties	Fe_3O_4	Al_2O_3	H_2O
k (W/mK)	9.7	40	0.613
C_p (J/kgK)	670	765	4179
ρ (kg/m^3)	5180	3970	997.1
σ (Ω^{-1}/m)	25×10^3	35×10^6	5×10^{-2}
Pr	–	–	6.2

It is not possible to find an analytical solution to these equations since they are non-linear. Therefore, the Equations (3.1) to (3.3) that were presented before, in addition to the boundary conditions, may be simplified to nine first-order equations. Let

$$f = y(1), \quad f' = y(2), \quad f'' = y(3), \quad g = y(4), \quad g' = y(5),$$
$$\theta = y(6), \quad \theta' = y(7), \quad \phi = y(8), \quad \phi' = y(9). \tag{3.5}$$

As a result, Equations (3.1) to (3.4) reduce to

$$f''' = \left(\frac{1+\beta}{\beta}\right)\left(\frac{l_1}{l_4}\right)\left[y(2)^2 - y(1)y(3) - 2\lambda y(4)\right] + \left(\frac{l_5}{l_4}\right)\frac{M}{1+m^2}\left(y(2) - my(4)\right), \tag{3.6}$$

$$g'' = \left(\frac{1+\beta}{\beta}\right)\left(\frac{l_1}{l_4}\right)\left[y(2)y(4) - y(1)y(5) + 2\lambda y(2)\right] + \left(\frac{l_5}{l_4}\right)\frac{M}{1+m^2}\left(y(4) + my(2)\right), \tag{3.7}$$

$$\theta'' = -\frac{1}{1+\frac{Rd}{l_3}\left[1+(\theta_w-1)y(6)\right]^3}\left[\Pr\frac{l_2}{l_3}y(1)y(7) + \frac{3Rd}{l_3}\left[1+(\theta_w-1)y(6)\right]^2(\theta_w-1)y(7)^2\right.$$
$$\left. + \frac{l_5}{l_3}MEc\Pr\left(y(2)^2 + y(4)^2\right) - \frac{\Pr}{l_3}Qy(6) + \frac{\Pr}{l_3(\rho C_p)_f}\left(Nt\,y(7)^2 + Nb\,y(9)y(7)\right)\right], \tag{3.8}$$

$$\phi'' = -\frac{Sc}{l_6}\left[y(1)y(9) - Rc\,y(8) + Sr\,\theta''\right] - \frac{1}{l_6}\frac{Nt}{Nb}\theta''. \tag{3.9}$$

with the boundary conditions

$$y_a(1) = 0, \quad y_a(2) = 1, \quad y_a(4) = 0, \quad y_a(6) = 1, \quad y_a(8) = 1, \tag{3.10}$$
$$y_b(2) = 0, \quad y_b(4) = 0, \quad y_b(6) = 0, \quad y_b(8) = 0, \tag{3.11}$$

Where, ya and yb characterize the operations comparing to their separate conditional variables considered at $\eta = 0$ and $\eta = \infty$ respectively. (3.6) to (3.9) along with boundary conditions given in (3.10) are decrypted numerically employing RK strategy with BVP-5C shooting strategy via user pleasant software MATLAB, that exhibits continuity over the interval $[0, \infty]$. During this procedure, the Equations (3.6) through (3.10) are first programmed in the MATLAB software, and the BVP-5C solver is then used to acquire the answers to these equations. The method begins with an initial estimate that is supplied at the beginning grid points, and then it dynamically modifies the step size in order to obtain the degree of accuracy that is needed. The eventual count of grid points is decided by the BVP-5C solver in an iterative manner as it moves forward through the solution. Table 3 is a listing of the governing factors that are responsible for determining the solution. In this research, the findings obtained indicate the effect of dimensionless factors on flow velocity, temperature, concentration, skin friction factor, Nusselt and Sherwood numerals. These dimensionless parameters include thermophoresis, Brownian movement, Hall current, magnetic variable, and thermal radiation. The answer has a reliability rating of 10^{-6}.

Assessing the validity of the numerical investigation involves a comparison of the skin friction coefficient along the x-axis $f''(0)$ and y-axis $g'(0)$ across multiple rotation parameter (λ) values with those reported in previous literature.

TABLE 4. Comparison of $f''(0)$ and $g'(0)$ with previous studies.

λ	Mustafa et al. [15]		Abdel-Wahed [1]		Elsaid et al. [8]		Current Study	
	$f''(0)$	$g'(0)$	$f''(0)$	$g'(0)$	$f''(0)$	$g'(0)$	$f''(0)$	$g'(0)$
0.50	-1.13838	-0.51276	-1.13837	-0.51276	-1.13838	-0.51276	-1.138887	-0.513234
1.00	-1.32503	-0.83709	-1.32503	-0.83710	-1.32503	-0.83710	-1.324959	-0.837051
2.00	-1.65235	-1.28726	-1.65235	-1.28726	-1.65235	-1.28726	-1.652354	-1.287258

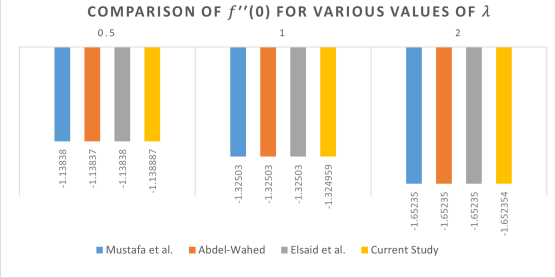

FIGURE 2. Comparison of $f''(0)$ for different values of λ with prior research outcomes.

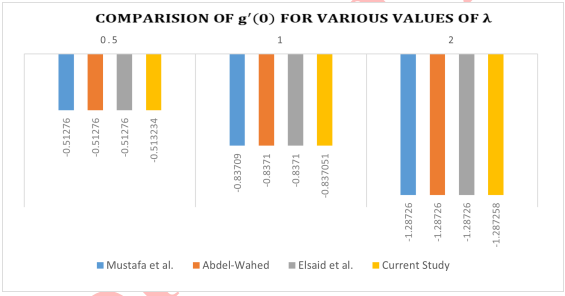

FIGURE 3. Comparison of $g'(0)$ for different values of λ with prior research outcomes.

TABLE 5. Comparison of $\dfrac{Nu_x}{\sqrt{Re}}$ with previous studies [8, 15].

Rd and θ_w	**Mustafa et al. [15]**	**Elsaid et al. [8]**	**Current Study**
$Rd = 0,\ \theta_w = 1$	1.85767	1.85678	1.792838
$Rd = 1,\ \theta_w = 1$	2.23985	2.23980	2.199043
$Rd = 1,\ \theta_w = 1.1$	2.30458	2.30660	2.270439
$Rd = 1,\ \theta_w = 1.5$	2.60934	2.60093	2.587576

Table 5 and the bar charts depicted in Figures 2 and 3 demonstrate the validation process of the current research in contrast to earlier studies conducted by Mustafa et al. [15], Abdel-Wahed [1] and Elsaid et al. [8] across various λ values. The latest findings indicate a strong agreement with the existing results, particularly under specific parameters when $M = m = \phi_1 = \phi_2 = Rd = \nu w = Ec = Sc = Rc = Nt = 0$ *and* $Nb = 0.0001$.

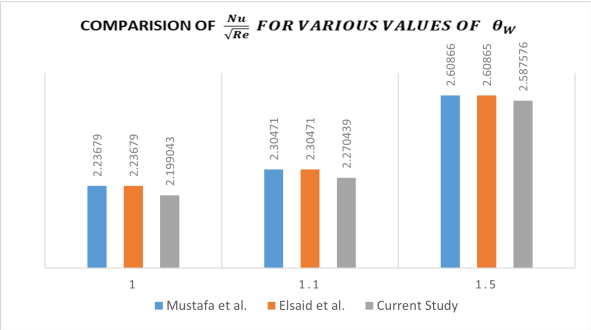

FIGURE 4. Comparison of $\frac{Nu_x}{\sqrt{Re}}$ for different values of θ_w with prior research outcomes.

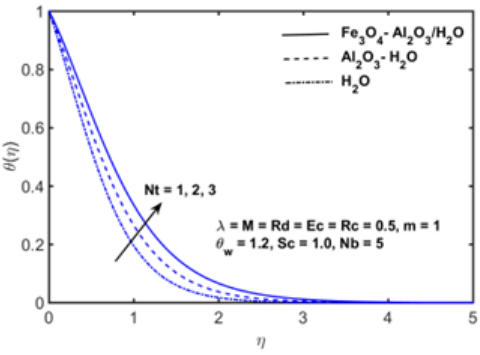

FIGURE 5. Effect of thermophoresis parameter (Nt) on $\theta(\eta)$.

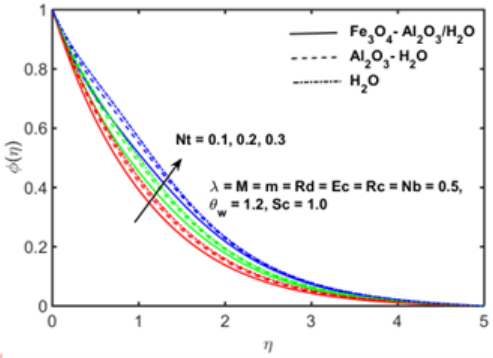

FIGURE 6. Effect of thermophoresis parameter (Nt) on $\phi(\eta)$.

4. Results and Discussion

This work examines the heat and mass transfer characteristics of MHD rotating hybrid nanofluid Fe_3O_4-Al_2O_3/H_2O flow over a three-dimensional linear stretching surface. A comparison has been showed among base fluid H_2O, Al_2O_3-H_2O nanofluid, and Fe_3O_4-Al_2O_3/H_2O hybrid nanofluid on velocity, temperature, and concentration fields under the influence of governing parameters, namely, thermophoresis ($0.1 \leq Nt \leq 3$), Brownian motion ($0.2 \leq Nb \leq 3$), Hall current ($0 \leq m \leq 2$), temperature ratio parameter ($1 \leq \theta_w \leq 2$), magnetic parameter ($0 \leq M \leq 1$), rotation parameter ($0 \leq \lambda \leq 1$), thermal radiation ($0.5 \leq Rd \leq 1.5$), Eckert number ($0.5 \leq Ec \leq 1.5$), Schmidt number ($0.5 \leq Sc \leq 1.5$), and chemical reaction parameter ($0.5 \leq Rc \leq 1.5$), involved in the problem. Figures 5 and 6 depict how the thermophoresis parameter (Nt) influences the temperature $\theta(\eta)$ and concentration $\phi(\eta)$ profiles of the three fluids, namely, Fe_3O_4-Al_2O_3/H_2O hybrid nanofluid, Al_2O_3-H_2O nanofluid, and the base fluid H_2O. The observations from these figures reveal that an increase in Nt results in a corresponding increase in both $\theta(\eta)$ and $\phi(\eta)$. Physically, elevating Nt results in an augmentation of the thermophoresis force, leading to nanoparticle movement from the heated region to the cooler one. This process results in an elevation of temperature and an increase in the thickness of the boundary layer, causing a simultaneous rise in both profiles. Moreover, it has been noted that the temperature profile of the hybrid nanofluid is elevated in comparison to both the nanofluid and the base fluid (water). Conversely, the concentration profile demonstrates a completely contrasting trend.

The distributions of $\theta(\eta)$ and $\phi(\eta)$ for hybrid nanofluid, nanofluid and base fluid are notably influenced by Brownian motion (Nb), as illustrated in Figures 7 and 8. An escalation in Nb values corresponds to an elevation in $\theta(\eta)$ and a reduction in $\phi(\eta)$. Physically, as Nb intensifies, the erratic movement of nanoparticles escalates, fostering

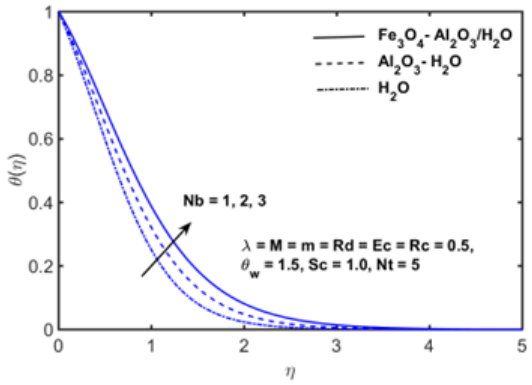

FIGURE 7. Effect of Brownian motion (Nb) on $\theta(\eta)$.

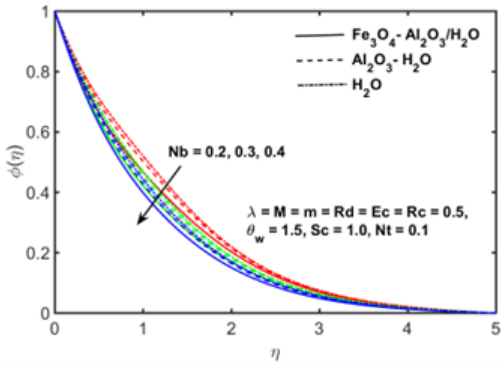

FIGURE 8. Effect of Brownian motion (Nb) on $\phi(\eta)$.

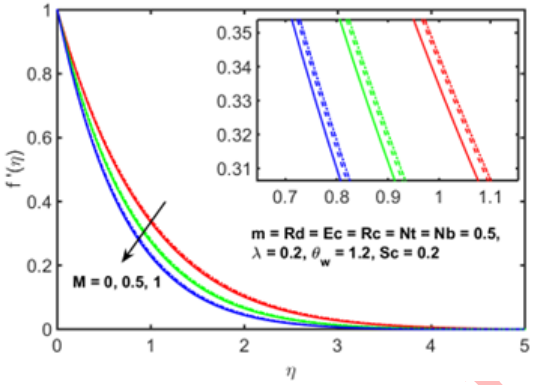

FIGURE 9. Effect of magnetic parameter (M) on $f'(\eta)$.

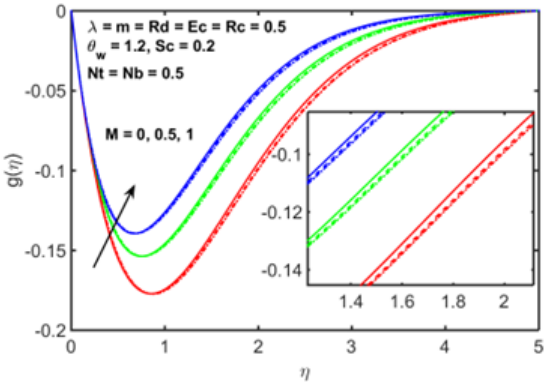

FIGURE 10. Effect of magnetic parameter (M) on $g(\eta)$.

heightened interactions among them. This transfer of kinetic significance through collisions from the microparticles to the liquid results in an augmented thermal boundary layer consistency, consequently elevating the temperature profile. Additionally, increased values of hinder the dispersion of nanoparticles from the designated region, leading to a persistent decline in concentration distribution. Similarly, it is marked that the temperature profile of the hybrid nanofluid is more increased than that of both the nanofluid and the base fluid. In contrast, the concentration profile of the base fluid surpasses that of both the nanofluid and the hybrid nanofluid.

Figures 9 to 11 illustrate the magnetic parameter (M) effects on the flow characteristics of hybrid nanofluid, nanofluid and base fluid. The plots depict velocity profiles along the x- and y-axes, represented by $f'(\eta)$ and $g(\eta)$, as well as the temperature profile $\Theta(\eta)$. As M increases, $f'(\eta)$ shows a decrease, while both $g(\eta)$ and $\Theta(\eta)$ exhibit an increase. As the magnetic field strength increases, the external force acting perpendicularly on the flowing fluid becomes more pronounced. Consequently, the Lorentz force, originating from the magnetic field, hinders and disrupts the movement of fluid particles. This effect results in a decrease in fluid velocity along the x-axis and an increase in velocity along the y-axis. Additionally, this force intensifies interactions within the magnetic domain, leading to an augmentation in both boundary layer thickness and reinforcement of the temperature profile. The hybrid nanofluid exhibits a higher temperature profile compared to both the nanofluid and the base fluid, while the velocity profile of water surpasses that of both the nano and hybrid nanofluid.

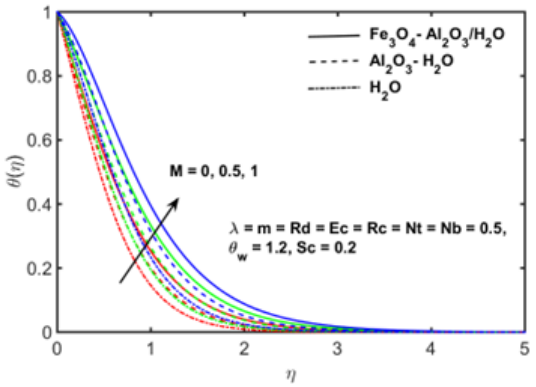

FIGURE 11. Effect of magnetic parameter (M) on $\theta(\eta)$.

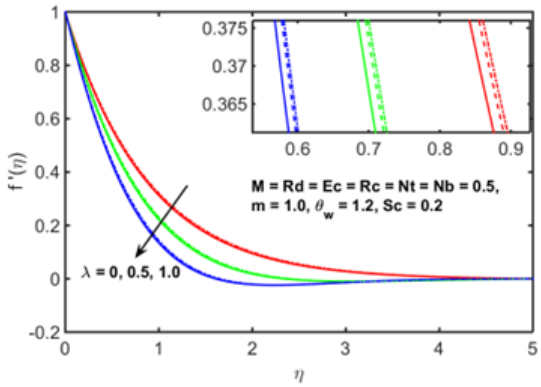

FIGURE 12. Effect of rotation parameter (λ) on $f'(\eta)$.

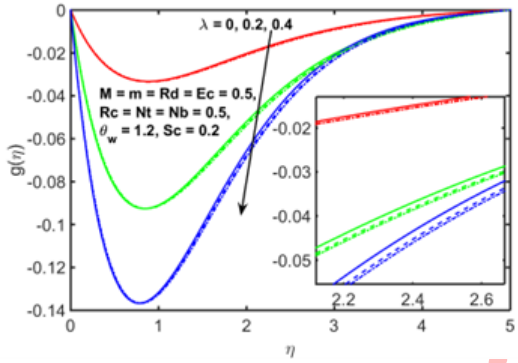

FIGURE 13. Effect of rotation parameter (λ) on $g(\eta)$.

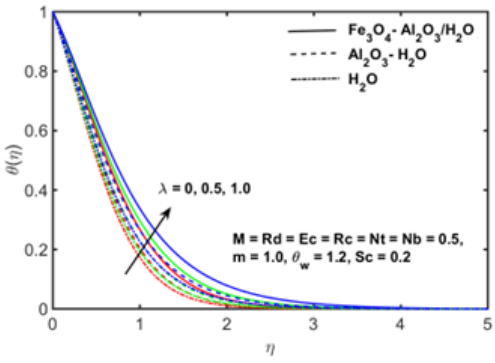

FIGURE 14. Effect of rotation parameter (λ) on $\theta(\eta)$.

The consequence of the rotation factor (λ) on the distributions of $f'(\eta), g(\eta) and \theta(\eta)$ is illustrated in Figures 12 and 14. Essentially, the rotation factor signifies the ratio of rotation rate to stretching rate. Higher values of λ denote a diminished stretching rate relative to the rotation rate, causing a reduction in the velocity profile along both the x- and y-axes. With the escalation of the rotation parameter, there is a concurrent rise in the kinetic energy of the fluid, leading to an increase in temperature. It is obeyed that the momentum profile along the y-axis and temperature distribution are higher for the hybrid nanoliquid, followed by the nanoliquid and the underneath fluid. Conversely, an opposing tendency is noted for the momentum profile along the x-axis

The significance of the Hall parameter, represented as m, becomes evident in the context of hybrid nanofluid flow, notably influencing $g(\eta)$ and $\theta(\eta)$ as depicted in Figures 15 and 16. An increase in the parameter m correlates with a decrease in $g(\eta)$ and an increase in $\theta(\eta)$. This behaviour can be ascribed to the diminishing value of $\frac{1}{1+m^2}$ as m rises. The decline in this value weakens the magnetic force, resulting in a diminished velocity profile along the y-direction. Analogous to the impact of a magnetic field, the Hall current effect introduces resistance, subsequently augmenting the thermal performance of the fluid flow. As a consequence, there is an observable rise in the temperature field. The profiles of $g(\eta)$ and $\theta(\eta)$ exhibit elevated levels in the $Fe_3O_4 - Al_2O_3/H_2O$ hybrid nanofluid compared to the $Al_2O_3 - H_2O$ nanofluid and base fluid H_2O, as per observations

Figures 17 and 18 represent the comparative numerical analysis of fluid dynamics, focusing on the temperature and concentration distributions for different fluids under varying heat source parameters. In Figure 17, the temperature

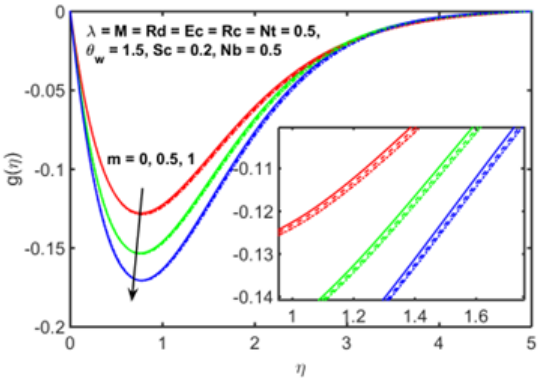

FIGURE 15. Effect of Hall current parameter (m) on $g(\eta)$.

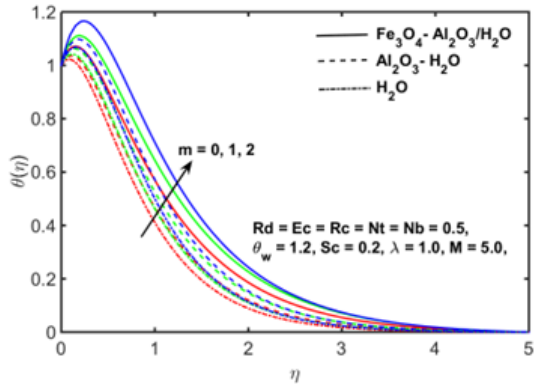

FIGURE 16. Effect of Hall current parameter (m) on $\theta(\eta)$.

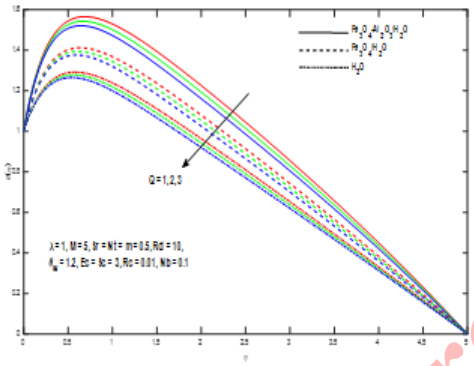

FIGURE 17. Effect of heat source parameter (Q) on $\theta(\eta)$.

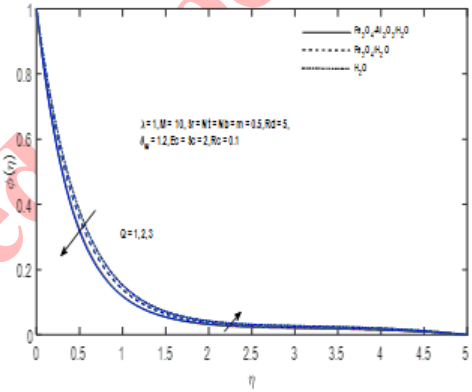

FIGURE 18. Effect of heat source parameter (Q) on $\phi(\eta)$.

distribution $\Theta(\eta)$ is shown for the same fluids, with the heat source parameter varied. The temperature increases with the rise in the heat source parameter for all the fluids. The hybrid nanofluid again demonstrates a higher temperature profile compared to both the nanofluid and the base fluid, signifying enhanced thermal conductivity due to the properties of the nanoparticles. In Figure 18, the concentration profile $\phi(\eta)$ is plotted for $Fe_3O_4 - Al_2O_3/H_2O$ hybrid nanofluid, Fe_3O_4/H_2O nanofluid, and pure H_2O as the base fluid, with the effects of the heat source parameter Q. As expected, with increasing heat source (Q), the concentration decreases for all fluids. The hybrid nanofluid $Fe_3O_4 - Al_2O_3/H_2O$ shows a higher concentration than the nanofluid Fe_3O_4/H_2O and the base fluid, indicating better mass transfer performance under the influence of thermophoresis and Brownian motion

Figures 19 and 20 illustrate the comparative behavior of the concentration ($\phi(\eta)$) and temperature ($\theta(\eta)$) profiles for various fluids, including $Fe_3O_4 - Al_2O_3/H_2O$ hybrid nanofluid, Fe_3O_4/H_2O nanofluid, and pure H_2O under the influence of the Soret (Sr) parameter. Figure 19 shows the temperature profile $\theta(\eta)$ for different fluids with varying values of the Soret number Sr. As the Soret number increases, the temperature profile rises, with the hybrid nanofluid exhibiting a higher temperature compared to the nanofluid and the base fluid. This indicates enhanced heat transfer in the hybrid nanofluid due to its superior thermal conductivity. The graph demonstrates that the Soret effect significantly influences the thermal behavior, especially for the hybrid nanofluid, resulting in an improved temperature distribution as compared to the other fluids. Figure 20 presents the concentration profile $\phi(\eta)$ for the same fluids,

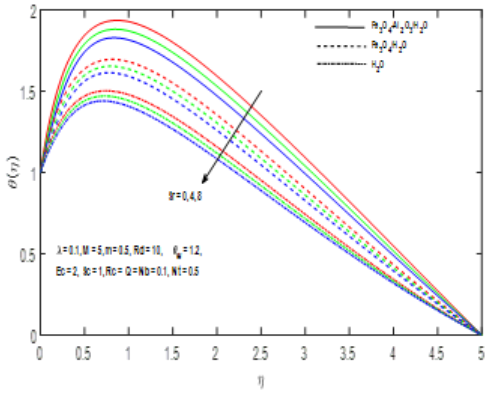

FIGURE 19. Effect of Soret parameter (Sr) on $\theta(\eta)$.

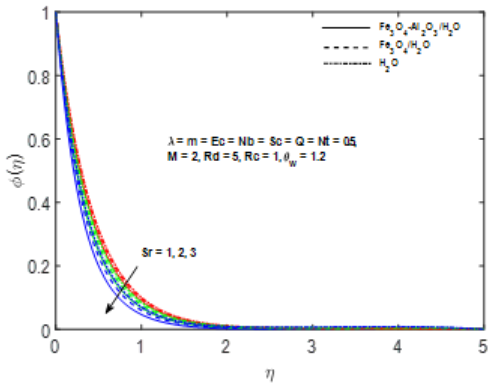

FIGURE 20. Effect of Soret parameter (Sr) on $\phi(\eta)$.

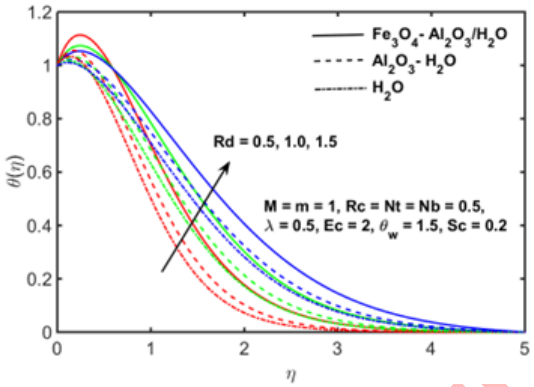

FIGURE 21. Effect of radiation parameter (Rd) on $\theta(\eta)$.

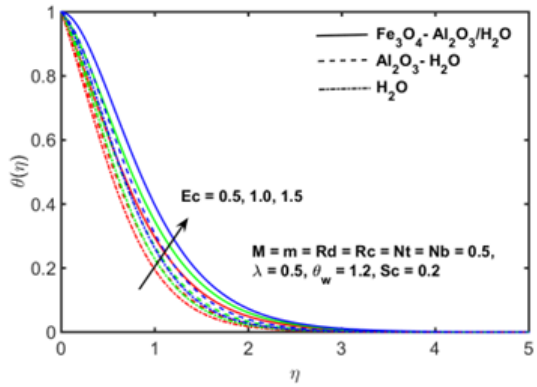

FIGURE 22. Effect of Eckert number (Ec) on $\theta(\eta)$

with varying Soret numbers. It is observed that as the Soret number increases, the concentration decreases for all fluids, with the hybrid nanofluid again showing a lower concentration profile than both the nanofluid and the base fluid. This suggests that the Soret effect reduces mass transfer efficiency, with the hybrid nanofluid demonstrating the most pronounced effect.

The temperature profile of three fluids exhibit a dual nature influenced by the radiation parameter (Rd), as depicted in Figure 21. For $0 < \eta < 1$, a decreasing trend in temperature is observed, while it increases for $\eta > 1$. Generally, radiation, deriving energy from liquid particles, serves as a method for heat transfer, generating heat energy in fluid motion and elevating temperature. In Figure 22, the impact of the Eckert number (Ec) on $\theta(\eta)$ is illustrated, where an increase in Ec results in elevated fluid temperature. This phenomenon is ascribed to the conversion of kinetic energy into internal energy, intensifying temperature distribution across the entire fluid region. The influence of the temperature ratio parameter (θ_w) on $\theta(\eta)$ is portrayed in Figure 23. The diagram demonstrates that as θ_w increases, both the temperature and the corresponding thermal boundary layer thickness experience augmentation. This occurrence is attributed to the fluid temperature rising significantly above the ambient temperature for elevated $\theta_w values$, leading to an elevation in the overall thermal condition of the fluid. Clearly, based on all the three figures, the temperature profile of $Fe_3O_4 - Al_2O_3/H_2O$ hybrid nanofluid surpasses that of $Al_2O_3 - H_2O$ nanofluid and base fluid H_2O. Figures 24 and 25 depict the influence of the Schmidt digit (Sc) and the chemical response (Rc) on the

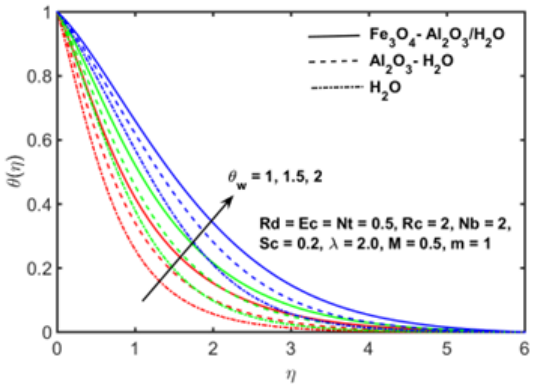

FIGURE 23. Effect of temperature ratio parameter (θ_w.) on $\theta(\eta)$

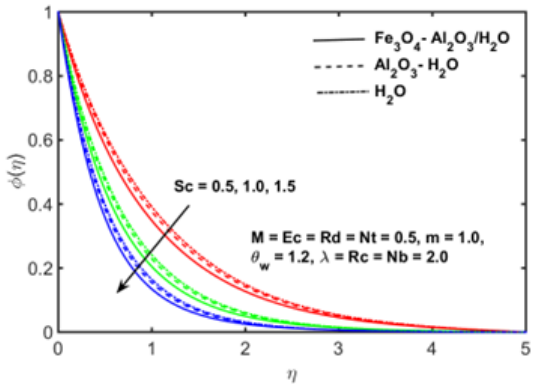

FIGURE 24. Effect of Schmidt number (Sc) on $\phi(\eta)$.

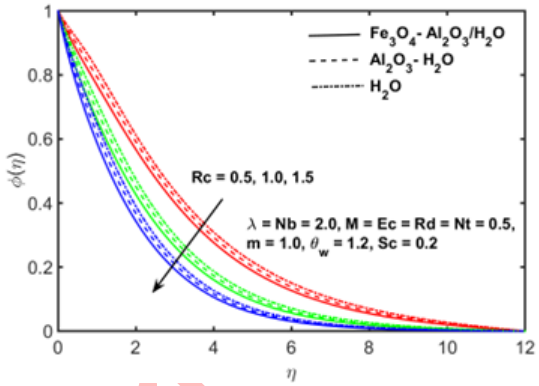

FIGURE 25. Effect of chemical reaction parameter (Rc) on $\phi(\eta)$.

concentration profile of three fluids. The Schmidt numeral, representing the relationship between speed and mass diffusivity, induces a reduction in diffusivity, subsequently causing a decrease in fluid concentration as Sc increases. Additionally, an augmentation in Rc leads to an accelerated utilization of nanomaterial's, resulting in a decline in $\phi(\eta)$. Evidently, from these two graphical representations, it is apparent that the concentration profile of the underpart liquid surpasses that of both the nanoliquid and hybrid nanoliquid.

During the computation of skin friction coefficients along the $x(\sqrt{Re}\ C_{fx})$ and $y(\sqrt{Re}\ C_{fy})$ axes, as well as the determination of local Nusselt $(Re^{-\frac{1}{2}}\ Nu)$ and Sherwood numbers $(Re^{-\frac{1}{2}}\ Sh)$, a consistent set of parameters was employed: $\phi_1 = 0.1,\ \phi_2 = 0.05, \lambda = 1,\ M = 0.5, Rd = 0.5, \nu w = 1.2, Ec = 0.5, Sc = 0.22, Rc = 0.5, Nt = Nb = 0.5, m = 2$. Notably, alterations to one parameter were made while holding all others constant throughout the analysis.

Table 6 presents data showcasing the impact of skin friction coefficient in both the x y directions, as well as the local Nusselt number and Sherwood number, concerning the leading non-dimensional parameters Nt, Nb, M, Rd and λ in this study. An increase in both M and λ results in a noticeable reduction in skin friction along both the x and y axes, whereas variations in the parameters Nt, Nb and Rd show no observable impact on skin friction. The local Nusselt number exhibits a downward trend with increasing values of Nt, Nb, M and λ, whereas a contrasting pattern is evident for Rd, which shows an increase, as these parameters rise. Further, the Sherhood number tends to rise as Nb, M, Rd and λ increase, conversely, it tends to decline as Nt increases.

TABLE 6. $\sqrt{Re}\ C_{fx}, \sqrt{Re}\ C_{fy}, Re^{-\frac{1}{2}}\ Nu_x$ and $Re^{-\frac{1}{2}}\ Sh_x$ impacts on the $Fe_3O_4 - Al_2O_3/H_2O$ hybrid nanofluid.

Nt	Nb	M	Rd	λ	$\sqrt{Re}\ C_{fx}$	$\sqrt{Re}\ C_{fy}$	$Re^{-1/2}Nu_x$	$Re^{-1/2}Sh_x$
0.1	–	–	–	–	-2.337435	-1.474208	1.307274	0.640240
0.2	–	–	–	–	-2.337435	-1.474208	1.307273	0.540703
0.3	–	–	–	–	-2.337435	-1.474208	1.307272	0.441166
–	5	–	–	–	-2.337435	-1.474208	1.307272	0.690009
–	10	–	–	–	-2.337435	-1.474208	1.307271	0.714893
–	15	–	–	–	-2.337435	-1.474208	1.307269	0.723188
–	–	1	–	–	-2.438539	-1.535690	0.480652	0.842306
–	–	1.1	–	–	-2.458267	-1.547693	0.321734	0.965652
–	–	1.2	–	–	-2.477843	-1.559606	0.164632	1.087649
–	–	–	0.5	–	-2.337435	-1.474208	1.307274	0.242091
–	–	–	1.0	–	-2.337435	-1.474208	1.442515	0.401867
–	–	–	1.5	–	-2.337435	-1.474208	1.552215	0.503883
–	–	–	–	0.5	-2.040109	-0.962424	1.407713	0.157392
–	–	–	–	1.0	-2.337506	-1.474241	1.304333	0.204008
–	–	–	–	1.5	-2.613530	-1.873264	1.200078	0.261482

5. CONCLUSION

This study investigates the dynamics of heat and mass transmission in a MHD rotating hybrid nanoliquid comprising $Fe_3O_4 - Al_2O_3$ particles suspended in water, flowing over a three-dimensional linear stretching surface. A comparative analysis has been conducted among three different fluid types: base fluid H_2O, $Al_2O_3 - H_2O$ nanofluid, $Fe_3O_4 - Al_2O_3/H_2O$ hybrid nanofluid on momentum, temperature and concentration disbandments underneath the consequence of controlling flow characteristics, namely, thermophoresis($0.1 \leq Nt \leq 3$), Brownian motion($0.2 \leq Nb \leq 3$), Hall current($0 \leq m \leq 2$), temperature ratio parameter($1 \leq \theta_w \leq 2$), magnetic parameter($0 \leq M \leq 1$), rotation factor($0 \leq \lambda \leq 1$), thermal radiation($0.5 \leq Rd \leq 1.5$), Eckert number($0.5 \leq Ec \leq 1.5$), Schmidt number($0.5 \leq Sc \leq 1.5$), chemical reaction parameter($0.5 \leq Rc \leq 1.5$), involving in the problem. BVP-5C shooting strategy is operated via MATLAB to decode the altered nonlinear ODEs controlling the liquid outpour. The outcomes of this investigation entail the subsequent conclusions:

- Augmenting the thermophoresis parameter (Nt) leads to elevated distributions of temperature ($\theta(\eta)$) and concentration ($\phi(\eta)$) across $Fe_3O_4 - Al_2O_3/H_2O$ hybrid nanofluid, $Al_2O_3 - H_2O$ nanofluid and the base fluid H_2O. Additionally, with increasing Nt values, there is a concurrent decrease observed in both the Nusselt and Sherwood numerals.
- An enhances in Brownian motion (Nb) values correlates with a rise in $\theta(\eta)$ and a decline in $\phi(\eta)$ across three distinct fluids. Additionally, there is an inverse relationship observed whereas the Nusselt numeral downhills with more elevated significances, the Sherwood numeral exhibits a corresponding increase.
- As the magnetic factor (M) rises, there is a diminishes in the velocity profile along the x-axis ($f'(\eta)$) and an increase along the y-axis ($g(\eta)$). Concurrently, the temperature profile experiences a rise with increasing M. Furthermore, as M increases, there is a decrease observed in both the skin friction along the x and y axes and the Nusselt number, while there is an increase in the Sherwood number.
- Increased values of the rotation parameter (λ) lead to a decrease in the velocity profile along both the x- and y-axes. Conversely, an inverse trend is noted in the temperature profile. With higher (λ) values, both the skin friction coefficient and the Nusselt number decrease, while the Sherwood number exhibits a contrasting pattern.
- For the three distinct fluids, an increase in the hall parameter (m) is associated with a reduction in $g(\eta)$ and a rise in $\theta(\eta)$. Higher values of temperature ratio parameter lead to an increase in the distribution of $\theta(\eta)$.

The temperature characteristics of these fluids exhibit a duality influenced by the radiation parameter (Rd). Within the range $0 < \eta < 1$, a downward trajectory in temperature is discernible, contrasting with the upward trend observed for $\eta > 1$.

- The temperature distribution of the $Fe_3O_4 - Al_2O_3/H_2O$ hybrid nanofluid exhibits a significant rise relative to the nanofluid $Al_2O_3 - H_2O$ and the base fluid H_2O for the parameters Nt, Nb, M, λ, m, Ec and θ_w. In contrast, the concentration gradient of the base fluid surpasses that of the nanofluid and hybrid nanofluid for the parameters Nt, Nb, Sc and Rc.
- In accordance with Karl Pearson's approach, the coefficient of correlation (r) reveals a perfect positive correlation, close to 1, between current and previous outcomes of Nusselt number $\frac{Nu_x}{\sqrt{Re}}$ values. This indicates a strong association between present and prior $\frac{Nu_x}{\sqrt{Re}}$ values as provided in [12].

Hybrid nanofluids such as $Fe_3O_4 - Al_2O_3/H_2O$ offer even broader prospects, notably in augmenting heat transfer, biomedical uses, cooling systems, and environmental remediation. These hybrid nanofluids not only diminish frictional resistance and drag but also serve in lubrication, hydraulic systems and cooling electronic devices. Furthermore, their utility extends to wastewater treatment, flow sensing, diagnostic imaging and purification procedures, illustrating their potential to transform fluid dynamics across multiple domains. Nanofluids, particularly those comprising $Al_2O_3 - H_2O$, are gaining increasing recognition for their capacity to improve heat transfer efficiency in diverse applications, while remaining both economical and safe. Their adaptability spans from enhancing the cooling of high-temperature electronic components to engine cooling, insulation, drug delivery, and water purification.

References

[1] M. S. Abdel-Wahed, *Rotating ferro-nanofluid over stretching plate under the effect of Hall current and Joule heating*, Journal of Magnetism and Magnetic Materials, *429* (2017), 287–293.

[2] F. Ahmad, S. Abdal, H. Ayed, S. Hussain, S. Salim, and A. O. Almatroud, *The improved thermal efficiency of Maxwell hybrid nanofluid comprising of graphene oxide plus silver/kerosene oil over stretching sheet*, Case Studies in Thermal Engineering, *27* (2021), 101257.

[3] A. M. Al-Hanaya, F. Sajid, N. Abbas, and S. Nadeem, *Effect of SWCNT and MWCNT on the flow of micropolar hybrid nanofluid over a curved stretching surface with induced magnetic field*, Scientific Reports, *10*(1) (2020), 1–18.

[4] Z. A. Alhussain and A. Tassaddiq, *Thin film blood based Casson hybrid nanofluid flow with variable viscosity*, Arabian Journal for Science and Engineering, (2021), 1–8.

[5] G. Aruna, K. Haribabu, B. Venkaeshwarlu, and K. Raghunath, *An unsteady MHD flow of a second-grade fluid passing through a porous medium in the presence of radiation absorption exhibits Hall and ion slip effects*, Heat Transfer, *52*(1) (2023), 780–806.

[6] K. N. V. C. Bhargava, S. M. Ibrahim, and K. Raghunath, *Magneto-hydrodynamic mixed convection chemically rotating and radiating 3D hybrid nanofluid flow through porous media over a stretched surface*, Mathematical Modelling and Numerical Simulation with Applications, *4*(4) (2024), 495–513.

[7] H. B. Kommaddi, K. Raghunath, C. Ganteda, and G. Lorenzini, *Heat and mass transfer on unsteady MHD chemically reacting rotating flow of Jeffrey fluid past inclined plates under the impact of Hall current, diffusion thermo and radiation absorption*, Journal of Advanced Research in Fluid Mechanics and Thermal Sciences, *111*(2) (2023), 225–241.

[8] E. M. Elsaid and K. S. Alshurafat, *Impact of Hall current and Joule heating on a rotating hybrid nanofluid over a stretched plate with nonlinear thermal radiation*, Journal of Nanofluids, *12*(2) (2023), 548–556.

[9] S. Hussain, V. V. L. Deepthi, V. O. Reddy, K. Raghunath, and L. Giulio, *Thermo-physical aspects of three dimensional non-newtonian Fe_3O_4/Al_2O_3 water based hybrid nanofluid with rotational flow over a stretched plate*, International Journal of Heat and Technology, *43*(1) (2025), 67–75.

[10] K. Jyothi, A. Sailakumari, V. R. Reddy, and K. Raghunath, *Neural network-assisted analysis of MHD boundary layer flow and thermal radiation effects on SWCNT nanofluids with Maxwellian and non-Maxwellian models*, Multiscale and Multidisciplinary Modeling, Experiments and Design, *8* (2025), 155.

[11] N. V. C. Katikala, C. Bhargava, M. I. Shaik, and K. Raghunath, *Effects of Hall current, radiation absorption and diffusion thermo on an unsteady MHD flow of second grade fluid through porous media in the presence of Joule heating and viscous dissipation*, Multiscale and Multidisciplinary Modeling, Experiments and Design, *8* (2025), 260.

[12] Y. S. Kumar, S. Hussain, K. Raghunath, F. Ali, K. Guedri, S. M. Eldin, and M. I. Khan, *Numerical analysis of magnetohydrodynamics Casson nanofluid flow with activation energy, Hall current and thermal radiation*, Scientific Reports, *13* (2023), 4021.

[13] B. Lavanya, J. G. Kumar, K. Raghunath, Y. R. Reddy, and M. J. Babu, *A comprehensive study of Carreau nanofluid flow over an inclined vertical plate with Cattaneo-Christov heat flux: numerical simulation and statistical analysis*, Radiation Effects and Defects in Solids, (2025), 1–18.

[14] L. A. Lund, Z. Omar, I. Khan, and E. S. M. Sherif, *Dual solutions and stability analysis of a hybrid nanofluid over a stretching/shrinking sheet executing MHD flow*, Symmetry, *12*(2) (2020), 276.

[15] M. Mustafa, A. Mushtaq, T. Hayat, and A. Alsaedi, *Rotating flow of magnetite-water nanofluid over a stretching surface inspired by non-linear thermal radiation*, PLoS ONE, *11*(2) (2016), e0149304.

[16] T. B. Omar, K. Raghunath, F. Ali, M. Khalid, E. S. M. Tag-ElDin, M. Oreijah, K. Guedri, N. B. Khedher, and M. I. Khan, *Hall current and Soret effects on unsteady MHD rotating flow of second-grade fluid through porous media under the influences of thermal radiation and chemical reactions*, Catalysts, *12* (2022), 1233.

[17] A. A. Pasha, M. K. Al Mesfer, M. W. Kareem, K. Raghunath, M. Danish, S. Patil, and V. R. Reddy, *Effects of rotational forces, and thermal diffusion on unsteady magnetohydrodynamic (MHD) flow of a viscoelastic fluid through porous media with isothermal inclined plates*, Case Studies in Thermal Engineering, *69* (2025), 105977.

[18] V. R. Prasad, N. U. B. Varma, B. Jamuna, M. S. Suresh, K. Sudhakaru, and K. Raghunath, *Effects of hall current and thermal diffusion on unsteady MHD rotating flow of water based Cu and TiO_2 nanofluid in the presence of thermal radiation and chemical reaction*, Multiscale and Multidisciplinary Modeling, Experiments and Design, *8* (2025), 161.

[19] K. Raghunath, V. Ramachandra Reddy, K. Haribabu, S. Noeiaghdam, and U. Fernandez-Gamiz, *Thermodynamic and buoyancy force effects of Cu and TiO_2 nanoparticles in engine oil flow over an inclined permeable surface*, Journal of King Saud University – Science, *36*(10) (2024), 103434.

[20] K. Raghunath, *Study of heat and mass transfer of an unsteady magnetohydrodynamic nanofluid flow past a vertical porous plate in the presence of chemical reaction, radiation and Soret effects*, Journal of Nanofluids, *12* (2023), 767–776.

[21] K. Raghunath and M. Ramana, *Hall, Soret, and rotational effects on unsteady MHD rotating flow of a second-grade fluid through a porous medium in the presence of chemical reaction and aligned magnetic field*, International Communications in Heat and Mass Transfer, *137* (2022), 106287.

[22] K. Raghunath, M. Ramana, N. Gulle, C. Ganteda, S. Ullah Khan, and M. I. Khan, *Hall and ion slip radiative flow of chemically reactive second-grade fluid through porous saturated space via perturbation approach*, Waves in Random and Complex Media, (2022), 1–17.

[23] K. Raghunath, C. Ganteda, and G. Lorenzini, *Effects of Soret, Rotation, Hall, and Ion Slip on Unsteady MHD flow of a Jeffrey fluid through a porous medium in the presence of heat absorption and chemical reaction*, Journal of Mechanical Engineering Research and Developments, *45*(3) (2022), 80–97.

[24] K. Raghunath, V. R. Reddy, M. I. Khan, S. S. Abdullaev, B. Habibullah, A. Boudjemline, M. Boujelbene, and Y. Bouazzi, *Unsteady magneto-hydrodynamics flow of Jeffrey fluid through porous media with thermal radiation, Hall current and Soret effects*, Journal of Magnetism and Magnetic Materials, *582* (2023), 171033.

[25] K. Raghunath, M. R. Ramana, V. R. Reddy, and M. Obulesu, *Diffusion thermo and chemical reaction effects on magnetohydrodynamic Jeffrey nanofluid over an inclined vertical plate in the presence of radiation absorption and constant heat source*, Journal of Nanofluids, *12* (2023), 147–156.

[26] K. Raghunath, M. R. Ravuri, V. Veeranna, M. I. Khan, S. Abdullaev, and N. Tamam, *Hall current and thermal radiation effects of 3D rotating hybrid nanofluid reactive flow via stretched plate with internal heat absorption*, Results in Physics, *53* (2023), 106915.

[27] K. Raghunath, M. R. Ramana, C. Ganteda, P. K. Chaurasiya, D. Tiwari, R. Kumar, D. Buddhi, and K. K. Saxena, *Processing to pass unsteady MHD flow of a second-grade fluid through a porous medium in the presence of radiation absorption exhibits diffusion thermo, Hall and ion slip effects*, Advances in Materials and Processing Technologies, *10*(2) (2023), 754–771.

[28] Y. S. Rani, P. K. Kumar, K. Raghunath, and F. Asmat, *Unsteady MHD rotating mixed convective flow through an infinite vertical plate subject to Joule heating, thermal radiation, Hall current, radiation absorption*, Journal of Thermal Analysis and Calorimetry, *149* (2024), 8813–8826.

[29] K. Raghunath, R. Sivaprasad, and G. S. S. Raju, *Hall effects on MHD convective rotating flow of through a porous medium past infinite vertical plate*, Annals of Pure and Applied Mathematics, *16* (2018), 353–263.

[30] K. V. Raju, M. R. Ramana, S. S. Reddy, and K. Raghunath, *Chemical radiation and Soret effects on unsteady MHD convective flow of Jeffrey nanofluid past an inclined semi-infinite vertical permeable moving plate*, Communications in Mathematics and Applications, *14*(1) (2023), 237–255.

[31] V. R. Reddy, G. Sreedhar, and K. Raghunath, *Effects of Hall current, activation energy and diffusion thermo of MHD Darcy-Forchheimer Casson nanofluid flow in the presence of Brownian motion and thermophoresis*, Journal of Advanced Research in Fluid Mechanics and Thermal Sciences, *105*(2) (2023), 129–145.

[32] V. R. Reddy, K. Raghunath, P. I. Khan, and K. Sudhakaru, *Thermo-physical and aligned magnetic field effects on unsteady MHD convection in Casson fluids over isothermal inclined plates in the presence of Joule heating and viscous dissipation*, Thermal Advances, *3* (2025), 100030.

[33] L. Zhang, V. R. Reddy, G. Aruna, B. Suneetha, and K. Raghunath, *3D-MHD mixed convection in a Darcy-Forchheimer Maxwell fluid: Thermo diffusion, diffusion-thermo effects, and activation energy influence*, Case Studies in Thermal Engineering, *61* (2024), 104916.

[34] D. Yadav, M. K. Awasthi, R. Ragoju, K. Bhattacharyya, K. Raghunath, M. Hassan, and J. Wang, *Impact of temperature-reliant thermal conductivity and viscosity variations on the convection of Jeffrey fluid in a rotating cellular porous layer*, Proceedings of Royal Society A, *480*(2301) (2024), 20240206.

[35] P. Sreedevi and P. S. Reddy, *Williamson hybrid nanofluid flow over swirling cylinder with Cattaneo–Christov heat flux and gyrotactic microorganism*, Waves in Random and Complex Media, – (2021), 1–28.

[36] M. Shoaib, M. A. Z. Raja, M. T. Sabir, S. Islam, Z. Shah, P. Kumam, et al., *Numerical investigation for rotating flow of MHD hybrid nanofluid with thermal radiation over a stretching sheet*, Scientific Reports, *10*(1) (2020), 1–15.

[37] M. Shoaib, M. A. Z. Raja, M. T. Sabir, M. Awais, S. Islam, Z. Shah, et al., *Numerical analysis of 3-D MHD hybrid nanofluid over a rotational disk in presence of thermal radiation with Joule heating and viscous dissipation effects using Lobatto IIIA technique*, Alexandria Engineering Journal, *60*(4) (2021), 3605–3619.

[38] N. C. Roy and I. Pop, *Flow and heat transfer of a second-grade hybrid nanofluid over a permeable stretching/shrinking sheet*, The European Physical Journal Plus, *135*(9) (2020), 1–19.

[39] S. Valiveti, M. Jetti, M. R. Yallalla, R. Kodi, and G. Lorenzini, *Analysis of heat and mass transfer in unsteady magnetohydrodynamic Casson fluid flow over isothermal inclined plates with thermal diffusion and heat source effects*, Power Engineering and Engineering Thermophysics, *3*(3) (2024), 195–208.

[40] V. V. L. Deepthi, M. A. M. Lashin, N. R. Kumar, K. Raghunath, F. Ali, M. Oreijah, K. Guedri, E. S. M. Tag-ElDin, M. I. Khan, and M. G. Ahmed, *Recent development of heat and mass transport in the presence of Hall, Ion Slip and Thermo Diffusion in radiative second grade material: application of micromachines*, Micromachines, *13* (2022), 1566.

[41] M. Obulesu, K. Raghunath, and R. Sivaprasad, *Hall current effects on MHD convective flow past a porous plate with thermal radiation, chemical reaction with radiation absorption*, AIP Conference Proceedings, *2246* (2020), 020003.